SUPPLEMENTARY INFORMATION

Theoretical Analysis of Optical and Thermoelectric Characteristics of Ti_nO_{2n-1}

S. Vahid Hosseini[1]; Mohaddeseh Abbasnejad[2]; Mohammad Reza Mohammadizadeh[1*],

[1] *Superconductivity Research Laboratory (SRL), Department of Physics, University of Tehran, North Kargar Ave., P. O. Box 14395-547, Tehran, Iran.*

[2] *Department of interdisciplinary physics and technology, Faculty of advanced science and technology, Shahid Bahonar University of Kerman, Kerman, Iran*

***Corresponding Author:**

Mohammad Reza Mohammadizadeh,

Prof. of Physics,

Permanent address:

Director, Superconductivity and Supermaterials Research Laboratory (SRL),

Department of Physics, University of Tehran,

North Kargar Ave.,

P.O. Box 14395-547

Tehran,

IRAN

Tel: +98 21 61118611, 61118634, & 61118749

Fax: +98 21 88004781

zadeh@ut.ac.ir

S1. THE BAND STRUCTURE OF Ti_nO_{2n-1}

The band structures of Ti_nO_{2n-1} phases using PBE and PBE+*U* are given in Fig. S1. Accordingly, the bands cross the Fermi level with a relatively high slope in metallic phases, indicating the high velocity of Fermi electrons. For the case of semiconducting phases, the bands near the Fermi level are typically flat, demonstrating the high electron effective mass, which is favorable in thermoelectric properties.

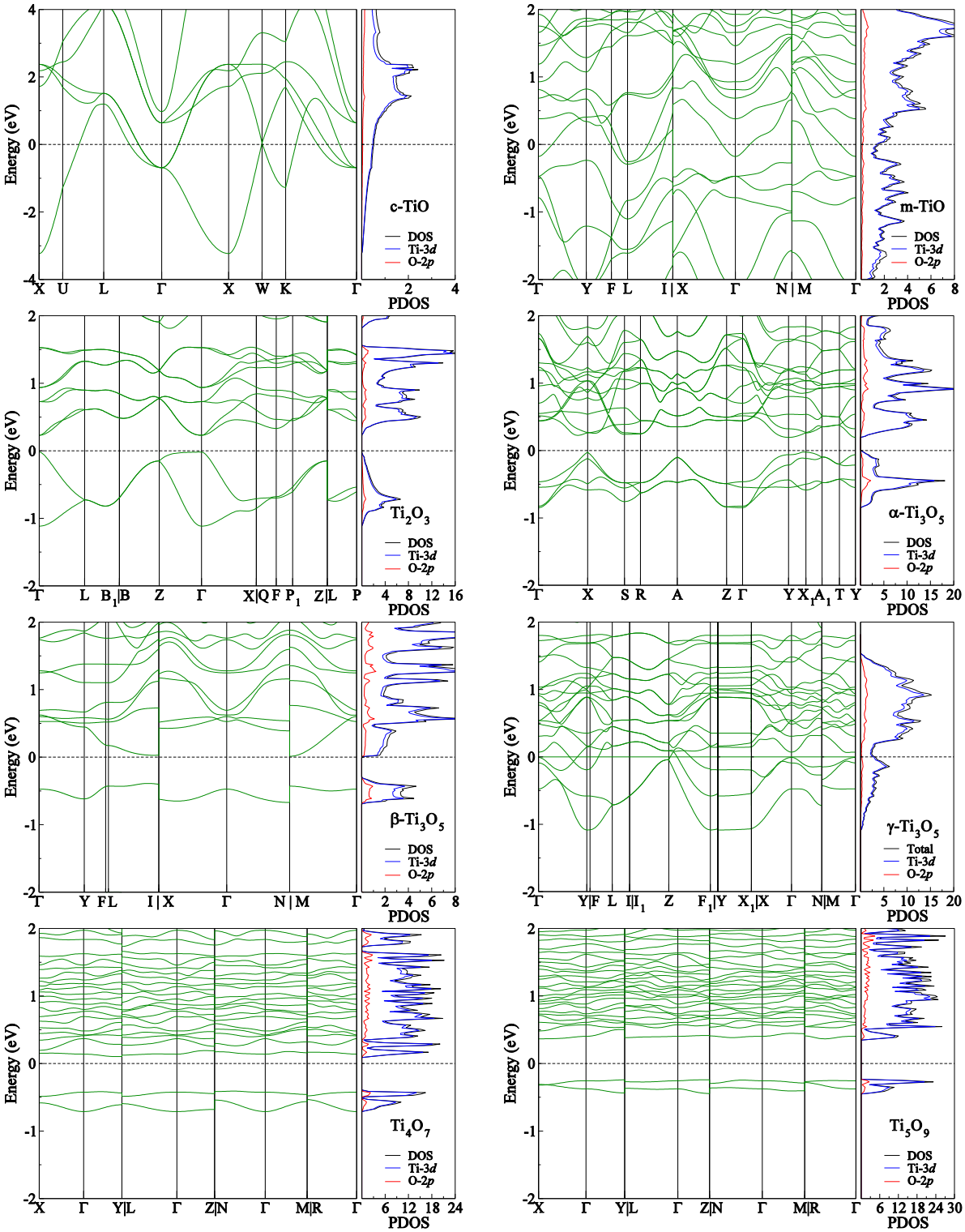

FIG. S1. Electronic band structure and density of states of Ti_nO_{2n-1} phases. Fermi level is at zero energy (The labeling of high symmetry points over the respective first BZ follows Setyawan et al. [1]).

S2. THE REAL AND IMAGINARY PART OF THE DIELECTRIC FUNCTION OF Ti_nO_{2n-1} USING PBE AND PBE+*U*

The real and imaginary parts of the dielectric function within PBE and PBE+*U* functionals are presented in Fig. S2. The imaginary part of the dielectric function is calculated by FGR according to the Drude-Lorentz model and perturbation theory. Similar to YS-PBE0, the optical absorption in the visible region is rather low. Moreover, there are two main peaks observed in the infrared and ultraviolet energy regions in the imaginary part of the dielectric function for semiconducting phases.

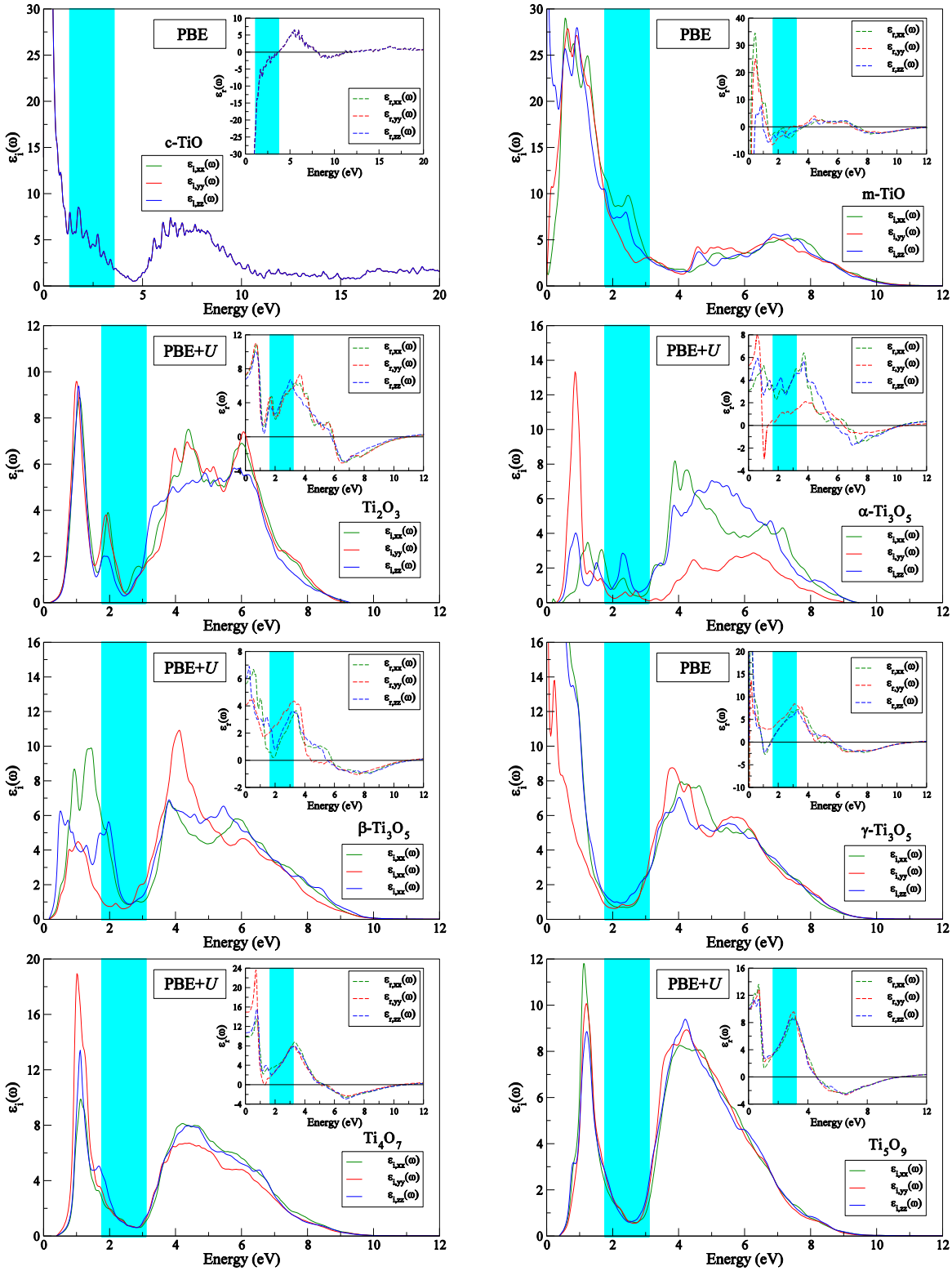

FIG. S2. Real and imaginary parts of the dielectric functions of Ti_nO_{2n-1} phases using PBE and PBE+*U* functionals. The visible region is shown by the sky blue color.

S3. THE OPTICAL CONDUCTIVITY OF Ti_nO_{2n-1} USING mBJ, PBE, YS-PBE0, and PBE+*U*

The real part of optical conductivity ($\sigma_r(\omega)$) as a function of incident photon energy was computed using different functionals for Ti_nO_{2n-1} phases as presented in Fig. S3. A similar trend is observed in the optical conductivity of Ti_nO_{2n-1} phases for metallic (using mBJ and PBE functionals) and semiconducting (using YS-PBE0 and PBE+*U* functionals). Ti_nO_{2n-1} phases have a relatively pronounced optical conductivity in the ultraviolet region, whereas it is weak in the visible range. According to Fig. S3, comparing the obtained results for Ti_2O_3 with the available experimental report [2] reveals that YS-PBE0 is more promising compared to PBE+*U*.

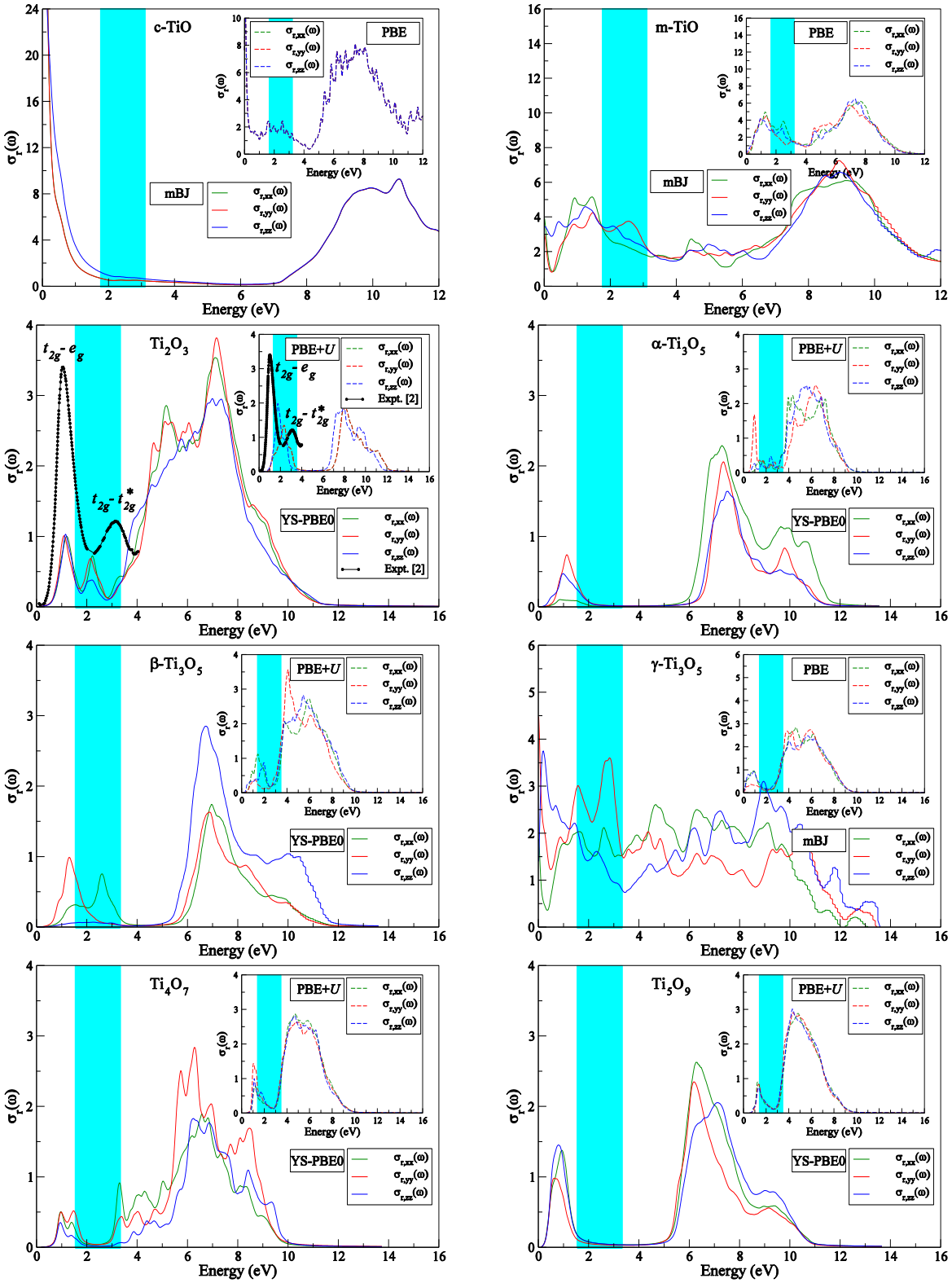

FIG. S3. Optical conductivity of Ti_nO_{2n-1} phases using mBJ, PBE, YS-PBE0, and PBE+*U* functionals. The visible region is shown by the sky blue color.

S4. THE REFLECTIVITY OF Ti_4O_7 USING YS-PBE0

The calculated reflectivity of Ti_4O_7 in both LT and HT phases are presented in Fig. S4 using the YS-PBE0 method. Moreover, the experimental results of reflectivity [3] at 6 K and 300 K related to LT and HT phases, respectivley are depicted as the insets of Fig. S4. As observed, YS-PBE0 results can follow the general trend for both LT and HT phases very well. This confirms that the results of YS-PBE0 are more robust.

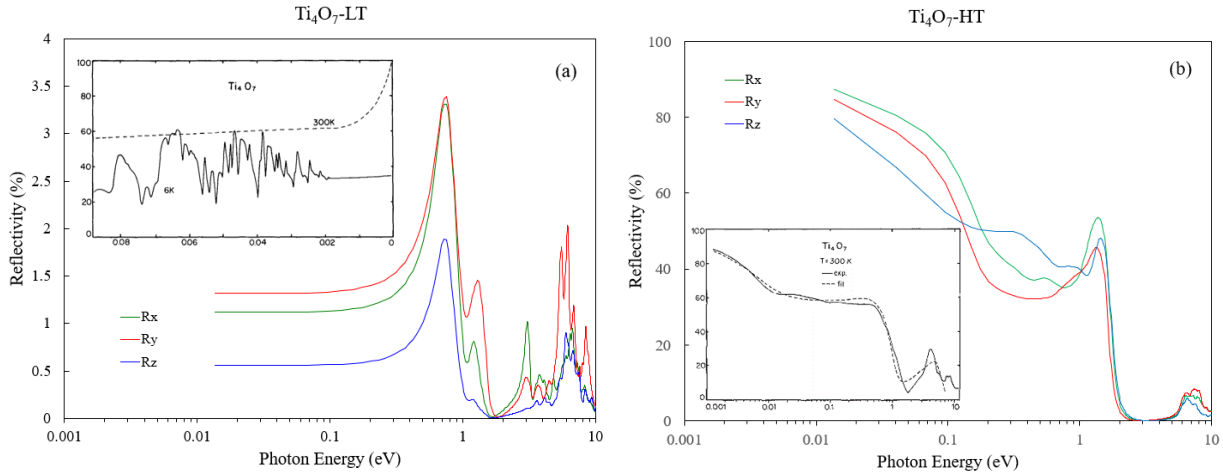

FIG. S4. The calculated reflectivity of (a): LT, and (b): HT phases of Ti_4O_7. The insets are experimental data extracted from Ref. [3].

S5. PHONON DISPERSION CURVES OF Ti_nO_{2n-1}

Figure S5 displays the phonon dispersion curves of the metallic and semiconducting phases of Ti_nO_{2n-1}. The stability of these structures is confirmed by the absence of any imaginary frequency modes in the entire BZ.

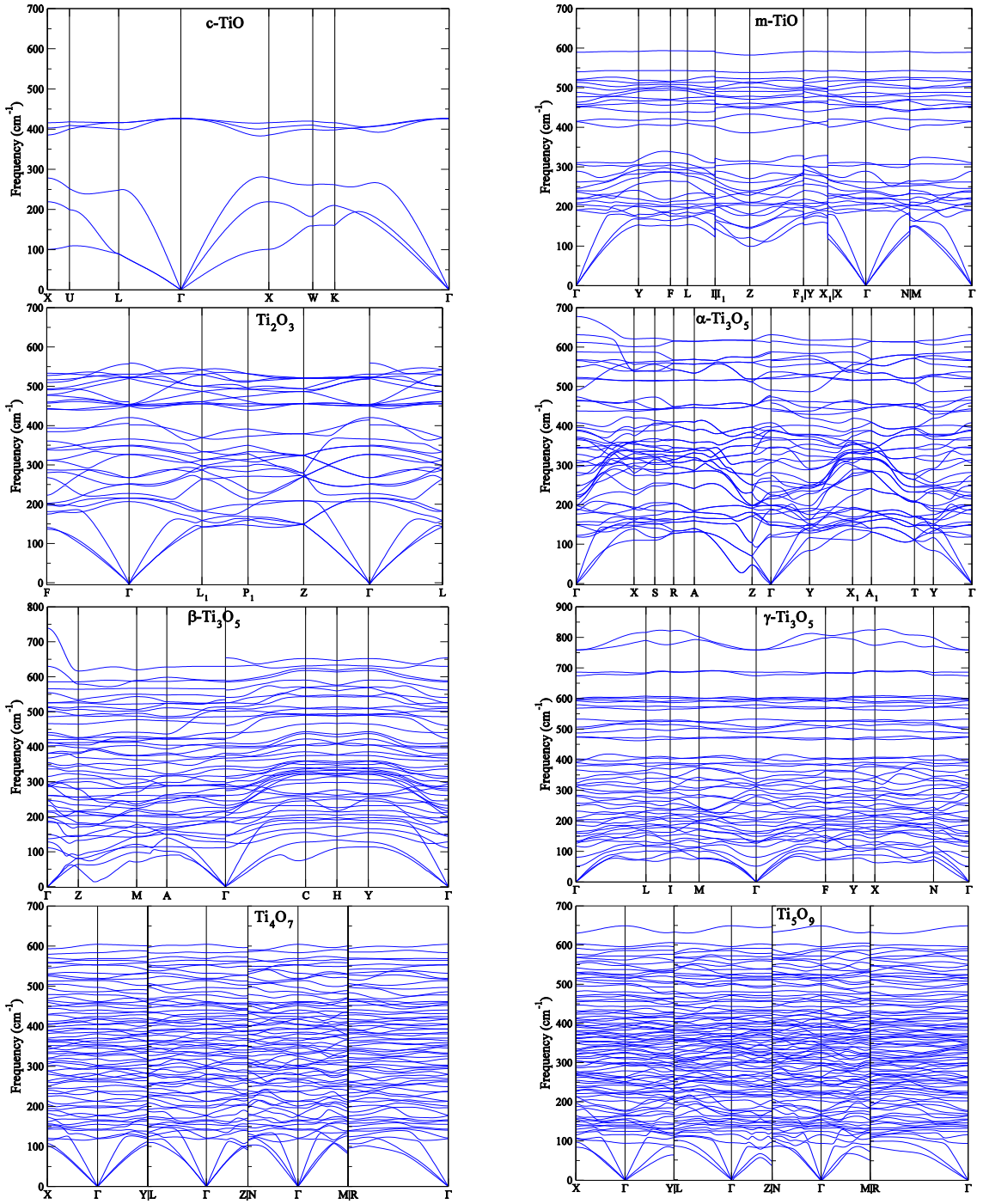

FIG. S5. The phonon dispersion curves of all phases of Ti_nO_{2n-1} using frozen phonon approach [4].

S6. PHONON SELF-ENERGY OF Ti_nO_{2n-1}

The imaginary part of the phonon self-energy versus frequency, calculated as described in Ref. [4], is shown for Ti_nO_{2n-1} structures (except Ti_5O_9) at different temperatures (300, 600, and 900 K), as illustrated in Fig. S6. This quantity is computed up to the second order in the anharmonic term of the external potential using many body perturbation theory, which is indicative of phonon-phonon interaction in the material. Moreover, as the temperature increases, more phonons are populated in the material. This increases the phonon population, leading to a higher probability of phonon-phonon interactions.

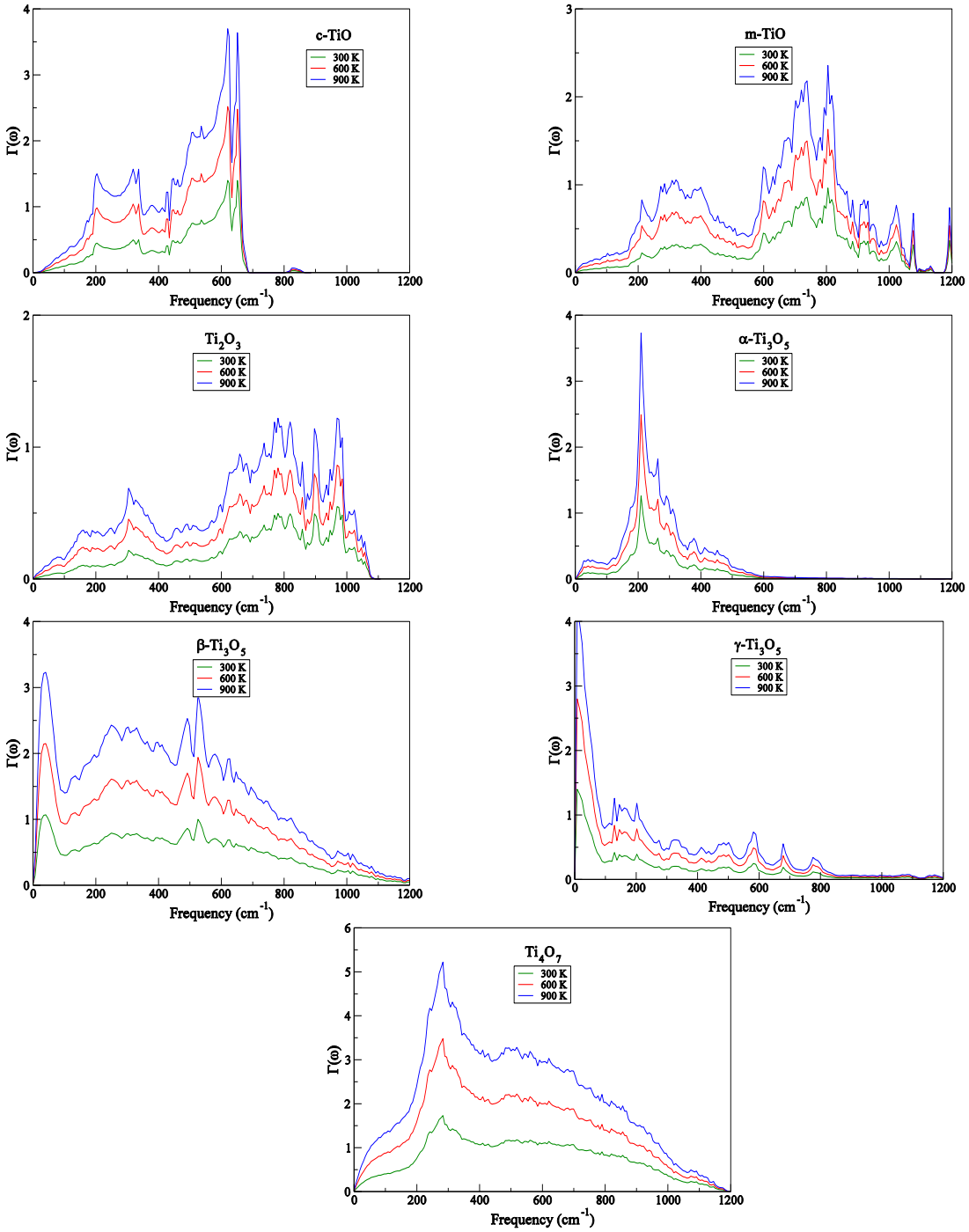

FIG. S6. The imaginary part of phonon self-energy vs. frequency for Ti_nO_{2n-1} structures (except Ti_5O_9) at different temperatures.

S7. THERMAL POWER FACTOR OF Ti_nO_{2n-1}

The PF/τ_e as a function of μ is shown for Ti_nO_{2n-1} structures at different temperatures (300, 600, and 900 K), as depicted in Fig. 15. The behavior of PF/τ_e versus temperature at zero doping is also shown as the insets in Fig. S7. Overall, PF/τ_e is increased by raising temperature at zero doping for all phases of Ti_nO_{2n-1}, having a good impact on the figure of merit. As it is depicted, *n* doping increases PF/τ_e in c-TiO dramatically, while PF/τ_e in m-TiO increases under both *n* or *p* doping. Also, PF/τ_e is increased almost symmetrically under *n* or *p* doping in the case of Ti_2O_3. Therefore, m-TiO and Ti_2O_3 can be favorable for thermoelectric switching devices. To use Ti_nO_{2n-1} materials practically in thermoelectric devices, doping level is significant. For instance, in Ti_2O_3, PF/τ_e reaches its maximum at μ~-0.25 eV. Additionally, *n*-type doping increases the PF/τ_e effectively in α-Ti_3O_5 and β-Ti_3O_5 phases. The lowest PF/τ_e is related to γ-Ti_3O_5 among Ti_3O_5 polymorphs that is due to the low values of both σ_e/τ_e and S_e in this phase. In the case of Magnéli phases, PF/τ_e has a negligible value below 300 K since there is no electrical conductivity below this temperature. Additionally, for Magnéli phases, PF/τ_e is effectively increased by *n* doping at high temperatures.

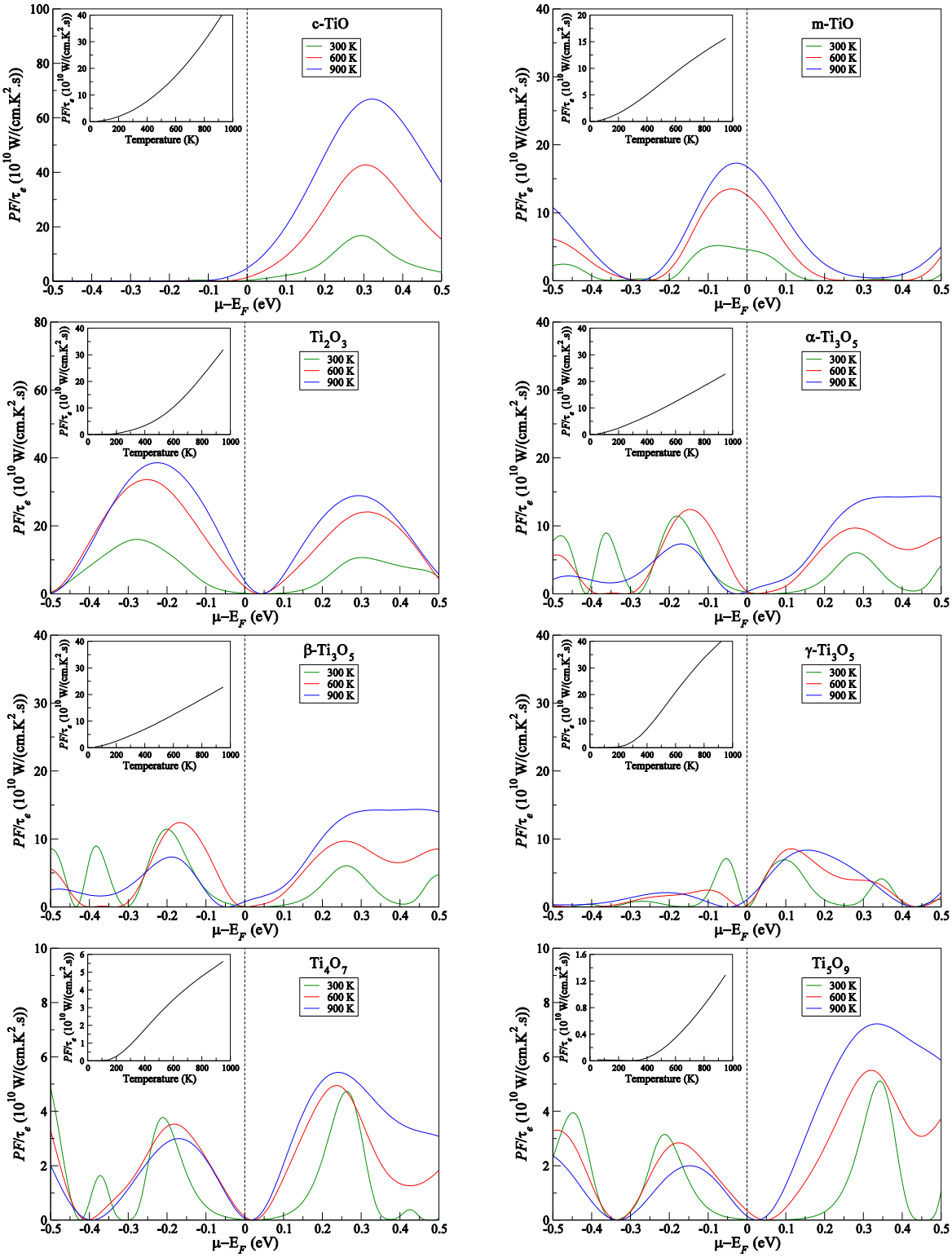

FIG. S7. The PF/τ_e as the function of chemical potential (μ) for Ti_nO_{2n-1}. The inset shows the variation of PF/τ_e versus temperature at zero doping.

REFERENCES

[1] W. Setyawan and S. Curtarolo, Computational materials science **49**, 299 (2010).
[2] M. Uchida, J. Fujioka, Y. Onose, and Y. Tokura, Physical review letters **101**, 066406 (2008).
[3] L. Degiorgi, P. Wachter, and C. Schlenker, Physica B: Condensed Matter **161**, 341 (1990).
[4] A. Togo, Journal of the Physical Society of Japan **92**, 012001 (2023).